Markus Braun
Peter Gilch
Wolfgang Zinth
Editors

BIOLOGICAL AND MEDICAL PHYSICS, BIOMEDICAL ENGINEERING

Ultrashort Laser Pulses in Biology and Medicine

Springer

BIOLOGICAL AND MEDICAL PHYSICS,
BIOMEDICAL ENGINEERING

BIOLOGICAL AND MEDICAL PHYSICS, BIOMEDICAL ENGINEERING

The fields of biological and medical physics and biomedical engineering are broad, multidisciplinary and dynamic. They lie at the crossroads of frontier research in physics, biology, chemistry, and medicine. The Biological and Medical Physics, Biomedical Engineering Series is intended to be comprehensive, covering a broad range of topics important to the study of the physical, chemical and biological sciences. Its goal is to provide scientists and engineers with textbooks, monographs, and reference works to address the growing need for information.

Books in the series emphasize established and emergent areas of science including molecular, membrane, and mathematical biophysics; photosynthetic energy harvesting and conversion; information processing; physical principles of genetics; sensory communications; automata networks, neural networks, and cellular automata. Equally important will be coverage of applied aspects of biological and medical physics and biomedical engineering such as molecular electronic components and devices, biosensors, medicine, imaging, physical principles of renewable energy production, advanced prostheses, and environmental control and engineering.

Markus Braun
Peter Gilch
Wolfgang Zinth
(Eds.)

Ultrashort Laser Pulses in Biology and Medicine

With 127 Figures

Springer

Dr. Markus Braun
Dr. Peter Gilch
Prof. Dr. Wolfgang Zinth
Ludwig-Maximilians-Universität München
Department für Physik, Lehrstuhl für BioMolekulare Optik
Oettingenstr. 67, 80538 München, Germany
E-mail: markus.braun@uni-muenchen.de
markus.braun@physik.uni-muenchen.de
peter.gilch@physik.uni-muenchen.de

Library of Congress Control Number: 2007933160

ISSN 1618-7210

ISBN-13 978-3-540-73565-6 Springer Berlin Heidelberg New York

Typesetting: Camera-ready by SPi Publisher Services, Pondicherry
Cover: eStudio Calamar Steinen

Printed on acid-free paper SPIN 12077311 57/3180/SPi - 5 4 3 2 1 0

Preface

During the last decade, the sources for ultrashort laser pulses developed from homebuilt prototype systems requiring tedious alignment by specialists into commercial turn-key products. Today they deliver laser pulses with durations of a few femtoseconds ($1\,\mathrm{fs} = 10^{-15}\,\mathrm{s}$) and cover a wide range of pulse energies and repetition rates. These light sources can roughly be divided into lasers and laser-amplifier combinations with subsequent nonlinear wavelength conversion. Femtosecond lasers typically feature pulse repetition rates of $\sim$100 MHz and pulse energies of up to $\sim$10 nJ in special spectral regions. They are very compact and reliable in operation. Laser-amplifier systems deliver much higher pulse energies in the millijoule range and above at repetition rates of typically 1 kHz. They are more complex in design and operation than femtosecond lasers. Nonlinear wavelength conversion by continuum generation or by optical parametric processes allows to cover the complete spectral range from the UV to the far infrared with femtosecond light pulses. The different types of femtosecond pulse sources have entered many areas of scientific research and technology. This book gives an overview of their application in biology and medicine.

A first important field of scientific application relies on the obvious property of femtosecond laser pulses, namely their short duration. It allows to trace even the fastest reactions in (bio)-molecules by means of time resolved spectroscopy. A great wealth of information on light-dependent biological processes such as photosynthesis, vision, and phototaxis has been obtained by means of femtosecond spectroscopy. The chapters by R. Diller, D.S. Larsen/R. van Grondelle/K.J. Hellingwerf, A.R. Holzwarth, M. Schmidt, T. Pullerits/T. Polivka/V. Sundström, and W. Zinth/J. Wachtveitl deliver important examples for the application of spectroscopy with highest temporal resolution in photobiology. The contribution of P. Hamm highlights the fact that these applications are not restricted to photobiology. Ultrashort IR pulses can help mapping out structural dynamics of biomolecules such as proteins and peptides in the electronic ground state.

Another type of application utilizes the high intensity of ultrashort laser pulses. Sources for ultrashort laser pulses feature high peak powers and low average power. This can facilitate strong nonlinear light matter interaction at a low thermal load. Nonlinear imaging and microscopy greatly profits from this property. Commonly, femtosecond lasers are employed for this purpose. Various examples for these applications can be found in the chapters by J.F. Bille, E. Haustein/P. Schwille, and A. Nimmerjahn/P. Theer/F. Helmchen. The high peak intensity of amplified pulses allows to manipulate biological tissue in a very controllable way. This paves the way to surgical applications which are summarized in the chapter by J.F. Bille.

A third type of application is based on the large bandwidth of ultrashort laser sources. The large bandwidth translates into short coherence lengths of the order of 1 µm. This coherence length defines the axial resolution in optical coherence tomography, an imaging tool particularly useful in ophthalmology. Principles and applications of this type of tomography are reviewed in the chapter by J.G. Fujimoto et al.

As this listing indicates, this book intends to give a broad overview of the topic. We have put certain emphasis on time-resolved spectroscopy since this area still dominates the applications of ultrashort laser pulses in biosciences – a judgment which might be biased a bit by the editors' research interests. This book is not intended to give a comprehensive description of the wide range of ultrashort pulses in biology and medicine. However we consider the contributions exemplary for various topics of this rapidly growing field. We hope that this book will promote the interest in this important research area.

Finally, we thank C. Ascheron from the Springer publishing house for the collaboration and all the colleagues for contributing their articles to the book and for their patience. Editing and publishing of a book usually takes longer than anticipated. This book is not an exception.

Munich
September 2007

M. Braun
P. Gilch
W. Zinth

Contents

Contributors

A. Aguirre
Department of Electrical Engineering and Computer Science and Research Laboratory of Electronics
77 Massachusetts Avenue
Building 36-345
Cambridge, MA 02139, USA
aaguirre@MIT.EDU

J.F. Bille
Kirchhoff-Institute for Physics
Im Neuenheimer Feld 227
D-69120 Heidelberg, Germany
josef.bille@urz.uni-heidelberg.de

Y. Chen
Department of Electrical Engineering and Computer Science and Research Laboratory of Electronics
77 Massachusetts Avenue
Building 36-345
Cambridge, MA 02139, USA
chen_yu@MIT.EDU

R. Diller
Fachbereich Physik, Technische Universität Kaiserslautern
Erwin Schrödinger Str. Geb. 46
67663 Kaiserslautern, Germany
diller@physik.uni-kl.de

J.G. Fujimoto
Department of Electrical Engineering and Computer Science and Research Laboratory of Electronics
77 Massachusetts Avenue
Building 36-345
Cambridge, MA 02139, USA
jgfuji@MIT.EDU

P. Hamm
Physikalisch Chemisches Institut
Universität Zürich
Winterthurerstr. 190
CH-8057 Zürich, Switzerland
phamm@pci.uzh.ch

E. Haustein
Biophysics Group
TU Dresden
Biotec
Tatzberg 47-51
D-01307 Dresden
elke.haustein@biotec.tu-dresden.de

F. Helmchen
Brain Research Institute, University of Zurich
Winterthurerstr. 190
CH-8057 Zurich, Switzerland
helmchen@hifo.unizh.ch

K.J. Hellingwerf
Laboratory for Microbiology
Swammerdam Institute for Life Sciences
University of Amsterdam
Nieuwe Achtergracht 166
1018 WS Amsterdam
The Netherlands
khelling@science.uva.nl

P. Herz
Department of Electrical Engineering and Computer Science and
Research Laboratory of Electronics
77 Massachusetts Avenue
Building 36-345
Cambridge, MA 02139, USA

A.R. Holzwarth
Max-Planck-Institut für
Bioanorganische Chemie
D-45470 Mülheim a.d. Ruhr
Germany

P.-L. Hsiung
Department of Electrical Engineering and Computer Science and
Research Laboratory of Electronics
77 Massachusetts Avenue
Building 36-345
Cambridge, MA 02139, USA

R. van Grondelle
Laboratory for Microbiology
Swammerdam Institute for Life Sciences, University of Amsterdam
Nieuwe Achtergracht 166
1018 WS Amsterdam
The Netherlands
rienk@nat.vu.nl

F. Kaertner
Department of Electrical Engineering and Computer Science and
Research Laboratory of Electronics
77 Massachusetts Avenue
Building 36-345
Cambridge, MA 02139, USA
kaertner@MIT.EDU

T. Ko
Department of Electrical Engineering and Computer Science and
Research Laboratory of Electronics
77 Massachusetts Avenue
Building 36-345
Cambridge, MA 02139, USA

D.S. Larsen
Department of Chemistry
University of California
Davis One Shields Avenue
Davis, CA 95616
dlarsen@ucdavis.edu

A. Nimmerjahn
Department of Biological Sciences and Applied Physics, James H. Clark Center for Biomedical Engineering and Sciences, Stanford University
318 Campus Drive
Stanford, CA 94305, USA

N. Nishizawa
Department of Electrical Engineering and Computer Science and
Research Laboratory of Electronics
77 Massachusetts Avenue
Building 36-345
Cambridge, MA 02139, USA

T. Polivka
Institute of Physical Biology
University of South Bohemia
Zamek 136
CZ-373 33 Nove Hrady
Czech Republic
polivka@umbr.cas.cz

T. Pullerits
Department of Chemical Physics
Lund University
Box 124
S-22100 Lund, Sweden
tonu.pullerits@chemphys.lu.se

M. Schmidt
Physics Department
University of Wisconsin-Milwaukee
1900 E. Kenwood Blv.
Milwaukee, WI 53221, U.S.A.
m-schmidt@uwm.edu

P. Schwille
BioTec TU Dresden
Institute for Biophysics
Tatzberg 47-51
D-01307 Dresden, Germany
schwille@biotec.tu-dresden.de

V. Sundström
Department of Chemical Physics
Lund University
Box 124
S-22100 Lund, Sweden
Villy.Sundstrom@chemphys.lu.se

P. Theer
Department Physiology and
Biophysics, University of Washington
1959 NE Pacific Street
Seattle, WA 98195, USA

J. Wachtveitl
Institute of Physical and Theoretical
Chemistry, Max von Laue-Strae 7
Institute of Biophysics, Max von
Laue-Strae 1, Goethe-Universitt
Frankfurt
60438 Frankfurt, Germany
wveitl@theochem.
uni-frankfurt.de

W. Zinth
CIPSM and Department für Physik
Ludwig-Maximilians-Universität
München
Oettingenstr. 67
80538 München, Germany
zinth@physik.uni-muenchen.de

Part I

Ultrafast Lasers in Medicine

1

Ultrahigh-Resolution Optical Coherence Tomography Using Femtosecond Lasers

J.G. Fujimoto, A.D. Aguirre, Y. Chen, P.R. Herz, P.-L. Hsiung, T.H. Ko, N. Nishizawa, and F.X. Kärtner

1.1 Introduction

Optical coherence tomography (OCT) is an emerging optical imaging modality for biomedical research and clinical medicine. OCT can perform high resolution, cross-sectional tomographic imaging in materials and biological systems by measuring the echo time delay and magnitude of backreflected or backscattered light [1]. In medical applications, OCT has the advantage that imaging can be performed *in situ* and in real time, without the need to remove and process specimens as in conventional excisional biopsy and histopathology. OCT can achieve axial image resolutions of 1 to 15 μm; one to two orders of magnitude higher than standard ultrasound imaging. The image resolution in OCT is determined by the coherence length of the light source and is inversely proportional to its bandwidth. Femtosecond lasers can generate extremely broad bandwidths and have enabled major advances in ultrahigh-resolution OCT imaging. This chapter provides an overview of OCT technology and ultrahigh-resolution OCT imaging using femtosecond lasers.

OCT was first demonstrated in 1991 [1]. Imaging was performed *in vitro* in the human retina and in atherosclerotic plaque as examples of imaging in transparent, weakly scattering media and in highly scattering media. *In vivo* OCT imaging of the human retina was demonstrated in 1993 [2, 3] and clinical studies in ophthalmology began in 1995 [4–6]. Since that time, OCT has emerged as an active area of research.

OCT imaging is analogous to ultrasound imaging, except that it uses light instead of sound. OCT performs cross-sectional imaging by measuring the time delay and magnitude of optical echoes at different transverse positions. The dimensions of the different structures can be determined by measuring the "echo" time it takes for light to be backreflected or backscattered from structures at various axial distances. Figure 1.1 shows how OCT images are generated. A cross-sectional image is generated by scanning the optical beam in the transverse direction and performing successive axial measurements [1]. This generates a two-dimensional array, which is a measurement

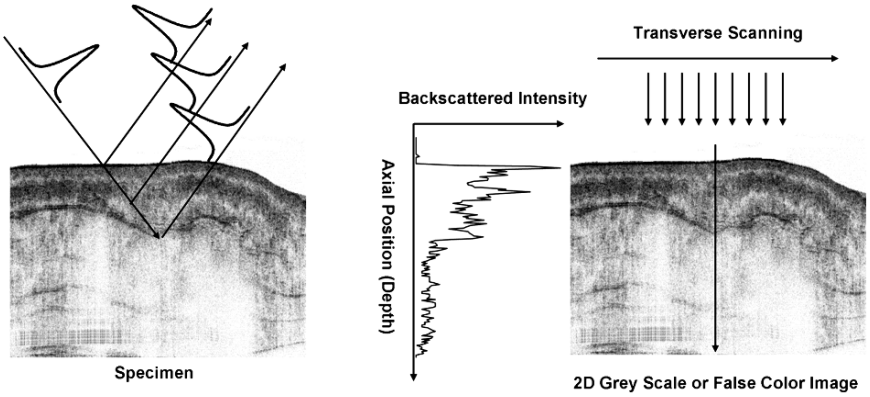

Fig. 1.1. OCT generates cross-sectional images by performing measurements of the echo time delay and magnitude of backscattered or backreflected light at different transverse positions. The two-dimensional data set can be displayed as a grey scale or false color image

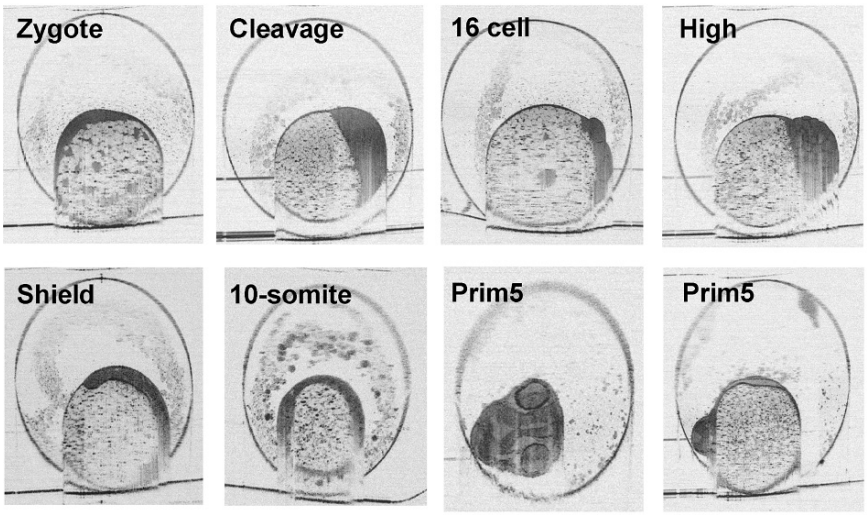

Fig. 1.2. OCT images of developing zebrafish egg. The OCT beam is incident from the top and successive axial measurements are performed at different transverse positions. These examples show ultrahigh-resolution OCT images displayed using a log grey scale. OCT has the advantage that it enables repeated imaging of the same specimen over time

of the backreflection or backscattering in a cross-sectional plane through the material or biological tissue.

Figure 1.2 shows an example of ultrahigh-resolution OCT images of a developing zebrafish egg. These images are performed on the same specimen

and demonstrate the ability of OCT to visualize structure noninvasively without the need to sacrifice and process specimens, as in conventional biopsy and histopathology. OCT image data are usually displayed as a two-dimensional grey scale or false color image. The vertical direction corresponds to the direction of the incident optical beam and the axial depth. The backscattered signal typically varies from approximately −50 dB (the maximum signal) to approximately −100 dB (the detection sensitivity limit). Because the signal varies over five orders of magnitude, it is convenient to use a log scale to display the image. The log display expands the dynamic range, but compresses relative variations in signal.

It is helpful to compare the characteristics of OCT, ultrasound, and microscopy imaging, as shown in Fig. 1.3. Ultrasound image resolution depends on the frequency or wavelength of the sound waves [7, 8]. Standard clinical ultrasound typically has a resolution of several hundred micrometers with image penetration depths of several centimeters. High-frequency ultrasound can have resolutions of several tens of micrometers and finer, but the imaging depth is very limited because of increased attenuation of high-frequency

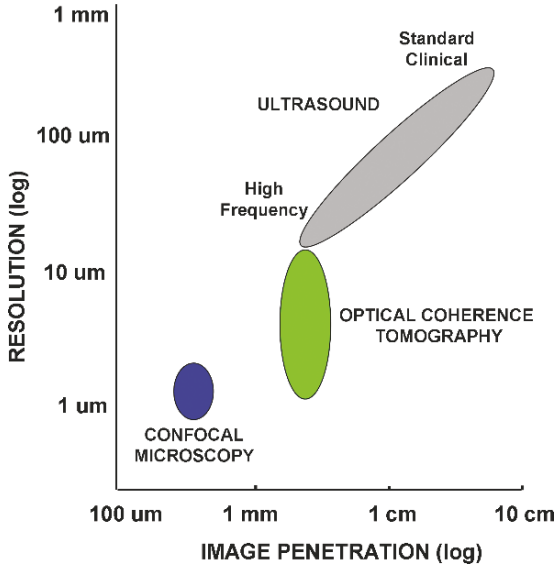

Fig. 1.3. Resolution and penetration depths for imaging with ultrasound, OCT, and confocal microscopy. For ultrasound imaging, higher frequencies yield improved resolution, but have increased ultrasonic attenuation, which limits image penetration depth. OCT has an axial image resolution from 1 to 15 µm, which is determined by the coherence length of the light source. In most biological tissues, attenuation from scattering limits OCT image penetration depth between 2 and 3 mm. Confocal microscopy has submicron transverse image resolution. However, the image penetration depth of confocal microscopy in biological tissues is limited to a few hundred micrometers

ultrasound in biological tissues. The axial resolution in OCT is determined by the coherence length of the light source and is independent of image penetration depth. Imaging depth is determined by attenuation from optical scattering and is typically 2 to 3 mm in most biological tissues [9–11]. OCT imaging has axial resolutions ranging from 1 to 15 μm, which is approximately 10 to 100 times finer than standard-resolution ultrasound imaging.

The high resolution of OCT enables imaging of features such as tissue architectural morphology or glandular organization. For medical applications, this enables the visualization and diagnosis of a wide range of pathologies. Because OCT is an optical technology, it can be integrated with instruments such as endoscopes, catheters, or laparoscopes that enable the imaging of internal organ systems.

1.2 Measuring Ultrafast Optical Echoes

In 1971, Michel Duguay first proposed the concept of using optical echoes to perform imaging in scattering systems such as biological tissue [12, 13]. This classic work demonstrated the use of an ultrafast optical Kerr shutter to photograph pulses of light in flight. The Kerr shutter is actuated by an intense, ultrashort light pulse that induces birefringence in an optical medium placed between crossed polarizers. The delay between the gating or reference pulse and the transient optical signal is adjusted to detect optical signals at various echo delays. Optical scattering limits imaging in biological tissues, and it was postulated that a high-speed shutter could be used to reject unwanted scattered light and detect light from internal tissue structures [12, 13]. High-speed optical gating might then be used to "see through" tissues and visualize pathology noninvasively.

Early studies also used nonlinear processes such as harmonic generation or parametric conversion for imaging and ranging in tissue [14–16]. The object or specimen is illuminated by short light pulses, and the backscattered or backreflected light is upconverted or parametrically converted by mixing with a reference pulse in a nonlinear optical crystal. The time delay and intensity of a high-speed optical signal can be measured using nonlinear optical gating. The time resolution is determined by the pulse duration, while the sensitivity is determined by the conversion efficiency of the nonlinear process. Optical ranging measurements have been demonstrated in biological tissues using femtosecond pulses and nonlinear intensity autocorrelation to measure structures such as the eye and in skin with axial resolutions of 15 μm [15]. Sensitivities of 10^{-7} can be achieved; however, this is still insufficient to image biological tissues, which have strong optical attenuation from scattering. Typical OCT systems that use low-coherence interferometry can achieve much higher sensitivities of 10^{-10}.

1.3 Low-Coherence Interferometry

Interferometry enables measurement of the echo time delay of backreflected or backscattered light with high sensitivity and high dynamic range. These techniques are analogous to coherent optical detection in optical communications. OCT is based on low-coherence interferometry or white light interferometry, a classic optical measurement technique first described by Sir Isaac Newton. Low-coherence interferometry has been applied to measure optical echoes and backscattering in optical fibers and waveguide devices [17–19]. The first studies using low-coherence interferometry in biological systems, to measure eye length, were performed in 1988 [20]. Measurements of corneal thickness were also demonstrated using low-coherence interferometry [21].

Figure 1.4 shows a schematic diagram of a Michelson interferometer. The measurement or signal beam $E_s(t)$ is reflected from the biological specimen or tissue being imaged, and a reference beam $E_r(t)$ is reflected from a reference mirror that is at a calibrated path length. The beams are interfered and a detector measures the intensity, or the square, of the electromagnetic field. The time delay that the optical beam travels in the reference arm can be controlled by varying the position of the reference mirror. Interference effects

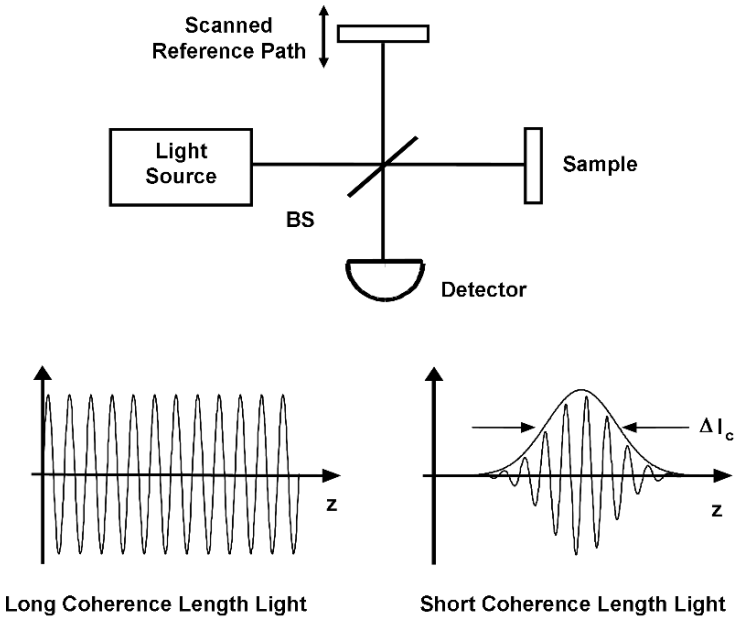

Fig. 1.4. OCT measures the echo time delay of light by using low-coherence interferometry. The OCT system is based on a Michelson-type interferometer. Backreflected or backscattered light from the tissue being imaged is correlated with light that travels a known reference path delay. Interferometric detection is sensitive to field rather than intensity and is analogous to optical heterodyne detection

will be observed in the intensity output of the interferometer, if the relative path lengths are changed by scanning the reference mirror. If the light source is highly coherent (narrow line width) with a long coherence length, then interference fringes will be observed for a wide range of relative path lengths of the reference and measurement arms. However, for applications in optical ranging or OCT, it is necessary to measure precisely the absolute distance and dimensions of structures within the material or biological tissue. In this case, light with a short coherence length (broad bandwidth) is used. Low-coherence light can be characterized as having statistical discontinuities in phase over a distance known as the coherence length. The coherence length is a measure of the coherence and is inversely proportional to the frequency bandwidth.

When low-coherence light is used as the source for the interferometer, interference is observed only when the path lengths of the reference and measurement arms are matched to within the coherence length of the light. If the path lengths differ by more than the coherence length, then the electromagnetic fields from the two beams are not correlated, and there is no interference. The interferometer measures the field autocorrelation of the light. In OCT imaging, the coherence length determines the axial or depth resolution. The magnitude and echo time delay of the reflected light can be measured by scanning the reference mirror position and demodulating the interference signal from the interferometer.

1.4 Resolution of OCT

The axial resolution in OCT imaging is determined by the coherence length of the light source. In contrast to standard microscopy, fine axial resolution in OCT can be achieved independent of the beam focusing conditions. The coherence length is proportional to the width of the field autocorrelation measured by the interferometer. The envelope of the field autocorrelation is equivalent to the Fourier transform of the power spectrum. Thus, the width of the autocorrelation function, or the axial resolution, is inversely proportional to the width of the power spectrum. For a Gaussian spectral distribution, the axial resolution Δz is: $\Delta z = (2 \ln 2/\pi)(\lambda^2/\Delta\lambda)$ where Δz and $\Delta\lambda$ are the full-widths-at-half-maximum of the autocorrelation function and power spectrum, respectively, and λ is the source center wavelength [22]. Since axial resolution is inversely proportional to the bandwidth of the light source, broad bandwidth optical sources are required to achieve high axial resolution.

The transverse resolution in OCT imaging is the same as in optical microscopy and is determined by the diffraction-limited spot size of the focused optical beam. The diffraction-limited minimum spot size is inversely proportional to the numerical aperture or the focusing angle of the beam. The transverse resolution is: $\Delta x = (4\lambda/\pi)(f/d)$, where d is the spot size on the objective lens and f is its focal length. Fine transverse resolution can be obtained by using a large numerical aperture that focuses the beam to a small spot size. At the same time, the transverse resolution is also related to the

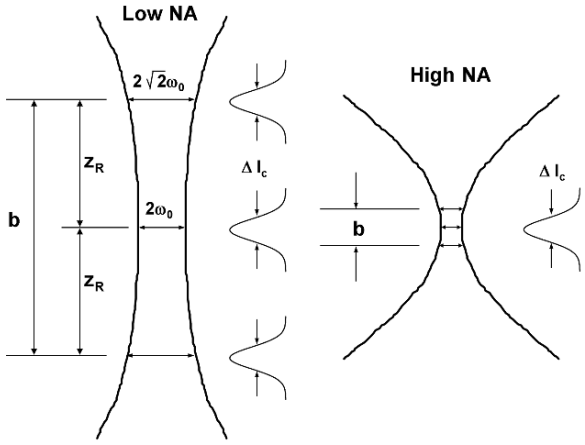

Fig. 1.5. Low and high numerical aperture (NA) focusing limits of OCT. There is a trade-off between transverse resolution and depth of field. OCT imaging is usually performed with low NA focusing, with the confocal parameter much longer than the coherence length. The high NA focusing limit achieves fine transverse resolution, but has reduced depth of field

depth of focus or the confocal parameter b, which is $2z_{\mathrm{R}}$, or two times the Rayleigh range: $2z_{\mathrm{R}} = \pi\Delta x^2/2\lambda$. Thus, increasing the transverse resolution produces a decrease in the depth of focus, which is similar to conventional microscopy.

Figure 1.5 shows schematically the relationship between focused spot size and depth of field for low and high numerical aperture focusing. Typically, OCT imaging is performed with low numerical aperture focusing to have a large depth of field. In this case, the confocal parameter is larger than the coherence length, $b > \Delta z$, and low-coherence interferometry is used to achieve axial resolution. The image resolution is determined by the coherence length in the axial dimension and the spot size in the transverse dimension. In contrast to conventional microscopy, OCT can achieve high axial resolution independent of the available numerical aperture. This feature is particularly powerful for applications such as ophthalmic imaging or catheter/endoscope imaging, where high numerical apertures are not available. However, operation with low numerical aperture also limits the transverse resolution because focused spot sizes are large.

It is also possible to perform OCT with high numerical aperture focusing and to achieve fine transverse resolutions. This results in a decreased depth of focus. This is the typical operating regime for microscopy or confocal microscopy. In this case, the depth of field can be shorter than the coherence length, $b < \Delta z$, and the depth of field can be used to differentiate backscattered or backreflected signals from different depths. This mode of operation is known as optical coherence microscopy (OCM) [23]. OCM has the advantage of achieving extremely fine transverse image resolution and is

useful for imaging scattering systems because the coherence gating rejects scattered light in front of and behind the focal plane more effectively than confocal gating alone.

1.5 Ultrahigh-Resolution OCT Using Femtosecond Lasers

The axial resolution in OCT imaging is determined by the bandwidth of the light source used for imaging. Compact superluminescent diodes (SLDs) have been used extensively in OCT systems. Ophthalmic OCT instruments use commercially available quantum-well SLDs that operate near 800 nm and typically generate output powers of a few milliwatts with bandwidths of 20 to 30 nm, thus yielding axial resolutions of ∼8 to 10 µm. Multiplexing SLDs at different wavelengths around 850 nm can achieve bandwidths approaching 150 nm; corresponding to axial resolutions of ∼3 µm. SLDs at 1.3 µm wavelengths can have output powers of 15 to 20 mW and bandwidths of 50 to 80 nm, which correspond to axial resolutions of ∼10 to 15 µm.

Femtosecond lasers are powerful light sources for ultrahigh-resolution OCT imaging because they can generate extremely broad bandwidths across a range of wavelengths in the near infrared. Figure 1.6 shows the axial resolution in air for optical bandwidths at center wavelengths of 800, 1 000, and 1 300 nm. These wavelengths can be generated using solid-state femtosecond lasers, such as the Ti:Al_2O_3, Nd:Glass or Yb fiber, and Cr:Forsterite lasers. The following sections describe examples of these femtosecond lasers and their application to ultrahigh-resolution OCT imaging.

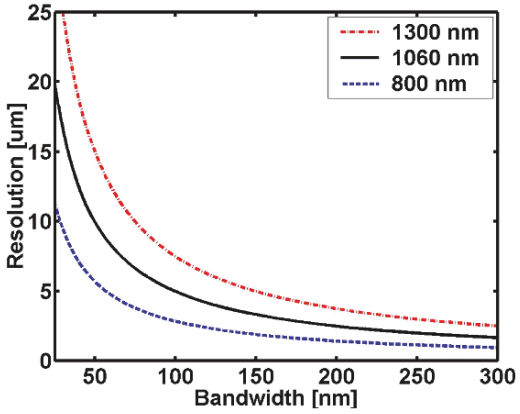

Fig. 1.6. Axial resolution vs. bandwidth of light sources for center wavelengths of 800, 1 000, and 1 300 nm. Micrometer-level axial resolution requires extremely broad optical bandwidths. Bandwidth requirements increase dramatically for longer wavelengths

1.6 Ultrahigh-Resolution OCT Imaging Using Ti:Al_2O_3 Femtosecond Lasers

The Kerr-lens modelocked (KLM) Ti:Al_2O_3 laser is the cornerstone for femtosecond optics and ultrafast phenomena. Early OCT imaging studies using Ti:Al_2O_3 lasers demonstrated axial image resolutions of $\sim$4 μm [24]. In the last few years, high-performance Ti:Al_2O_3 lasers have been made possible through the development of double-chirped mirror (DCM) technology [25–32]. DCMs can compensate high-order dispersion and have extremely broadband reflectivity, thus enabling the generation of few cycle optical pulses. In addition, DCMs enable dispersion compensation without the use of intracavity prisms, thereby greatly improving the stability and ease of use of femtosecond lasers. With these recent advances, Ti:Al_2O_3 lasers achieve pulse durations of $\sim$5 fs; corresponding to only two optical cycles and octave bandwidths at 800 nm [30, 33–35]. Using state-of-the-art Ti:Al_2O_3 lasers, OCT axial image resolutions of $\sim$1 μm have been demonstrated [36, 37].

Figures 1.7 and 1.8 show schematics of a femtosecond Ti:Al_2O_3 laser light source and an ultrahigh-resolution OCT system. The Ti:Al_2O_3 laser uses DCMs and intracavity prisms that enable the adjustment of intracavity dispersion. This laser generates pulses of $\sim$5.5 fs duration; corresponding to bandwidths of $\sim$300 nm centered at 800 nm with an average power of 150 mW. The output spectrum can be shaped using a spectral filter. The shape of the OCT axial point spread function depends on the Fourier transform of the optical spectrum. Therefore, a smooth spectrum without sharp edges or modulation is required to reduce side lobes or wings on the OCT axial point spread function.

Femtosecond pump–probe measurements require special techniques to minimize dispersion and maintain the femtosecond pulse duration at the sample. In contrast, OCT measurements do not require short pulse durations,

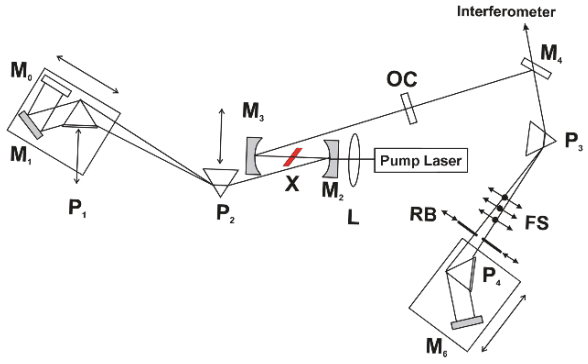

Fig. 1.7. Schematic of femtosecond Ti:Al_2O_3 laser using double-chirped mirror (DCM) technology. DCMs provide increased mirror bandwidth and compensation of higher order cubic dispersion. The laser combines DCMs and intracavity prisms to enable the fine-tuning of the dispersion operating point. From ref [28]

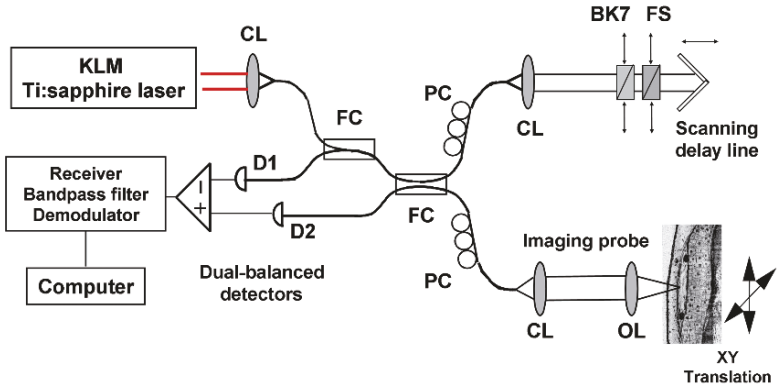

Fig. 1.8. Ultrahigh-resolution OCT system using a femtosecond Ti:Al_2O_3 laser light source. The interferometer is optimized to support broad bandwidths and dispersion is balanced between the sample and reference arms. From ref [36]

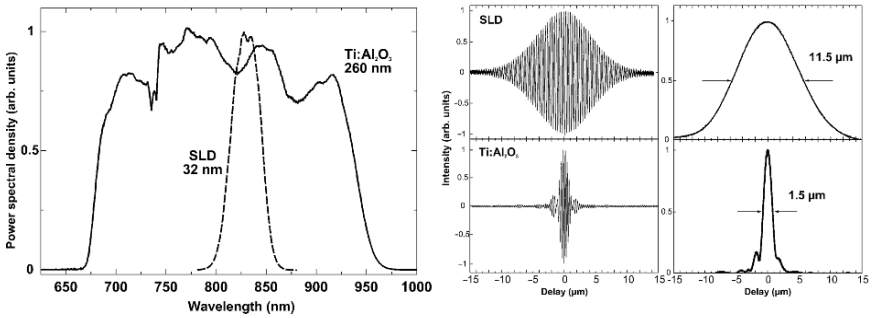

Fig. 1.9. OCT optical spectrum, interference signals, and point spread functions using femtosecond Ti:Al_2O_3 laser vs. a standard-resolution superluminescent diode (SLD). The femtosecond laser generates a bandwidth of 260 nm and achieves a free-space axial resolution of 1.5 µm. In contrast, the SLD generates a bandwidth of 32 nm and achieves a resolution of 11.5 µm. From ref [36]

because the axial image resolution depends on the field correlation and not the intensity correlation. Therefore, it is not necessary to compensate group velocity dispersion in the reference and signal paths of the interferometer. Instead, dispersion must be precisely balanced or matched in the two interferometer arms. In an ultrahigh-resolution OCT system, dispersion introduced by different fiber lengths and optics in the interferometer sample arm is matched using adjustable thickness fused silica (FS) and BK7 glass in the reference arm. Figure 1.9 shows a comparison of the optical bandwidth and interferometer output traces determining the axial resolution of a superluminescent diode (SLD) and the Ti:Al_2O_3 laser [36, 37]. Optical bandwidths of ∼260 nm are transmitted; corresponding to axial image resolution of ∼1 µm.

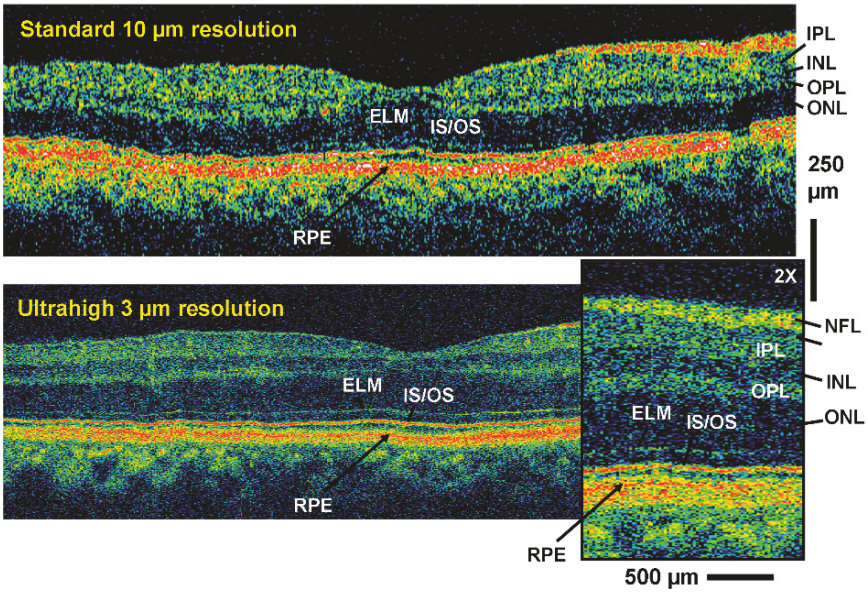

Fig. 1.10. Comparison of standard and ultrahigh-resolution OCT images of the normal human retina. The axial resolution is 10 µm using an SLD light source and 3 µm using a femtosecond laser light source. The ultrahigh-resolution OCT image enables visualization of all major retinal layers

OCT has been widely used in ophthalmology, where it is becoming a standard for clinical diagnosis and monitoring of retinal diseases such as macular holes, age-related macular degeneration, glaucoma, and diabetic retinopathy [4–6]. Figure 1.10 shows an example of ultrahigh-resolution OCT imaging of the human retina. The figure shows a comparison between standard OCT with 10 µm axial resolution performed using an SLD light source and ultrahigh-resolution OCT with ∼3 µm axial resolution performed using a femtosecond laser light source. The standard-resolution OCT image was acquired using a commercial ophthalmic OCT system (StratusOCT, Carl Zeiss Meditec). The axial resolution in the ultrahigh-resolution OCT image was limited by the ability to accurately compensate dispersion in the eye. Recent results that use more sophisticated OCT techniques have achieved axial resolutions as high as ∼2 µm in the retina. Measurements were performed with retinal exposures of <750 µW; within ANSI standards for safe retinal exposure and consistent with the exposure levels used in commercial OCT clinical instruments. To reduce the intensity of the femtosecond laser pulses, the light was first coupled into a 100 m length of optical fiber, thereby dispersively broadening the pulses to several hundred picoseconds in duration. Because of the high laser repetition rate of ∼100 MHz, individual pulses have very low

energies, and the light source can be considered a continuous-wave light source from the viewpoint of ocular safety.

The normal human retina has multiple layers. As shown in Fig. 1.10, standard-resolution OCT can visualize larger scale morphology, such as the retinal nerve fiber layer, retinal pigment epithelium, the inner and outer plexiform layers, and the inner and outer nuclear layers. Ultrahigh-resolution OCT offers an unprecedented resolution and can visualize almost all of the major retinal layers, including very fine structures such as the external limiting membrane and the inner and outer segments of the photoreceptors [37–39]. Changes in these intraretinal structures occur in a variety of retinal diseases, including age-related macular degeneration, diabetic retinopathy, and glaucoma.

Several research groups have begun studies of ultrahigh-resolution OCT in clinical ophthalmology. We have imaged more than 700 patients using an ultrahigh-resolution OCT prototype instrument at the New England Eye Center of the Tufts-New England Medical Center. Extensive studies have also been performed by W. Drexler and colleagues at the University of Vienna. Figure 1.11 shows an example of ultrahigh-resolution OCT imaging in a patient with a macular hole, which is a hole in the retina characterized by

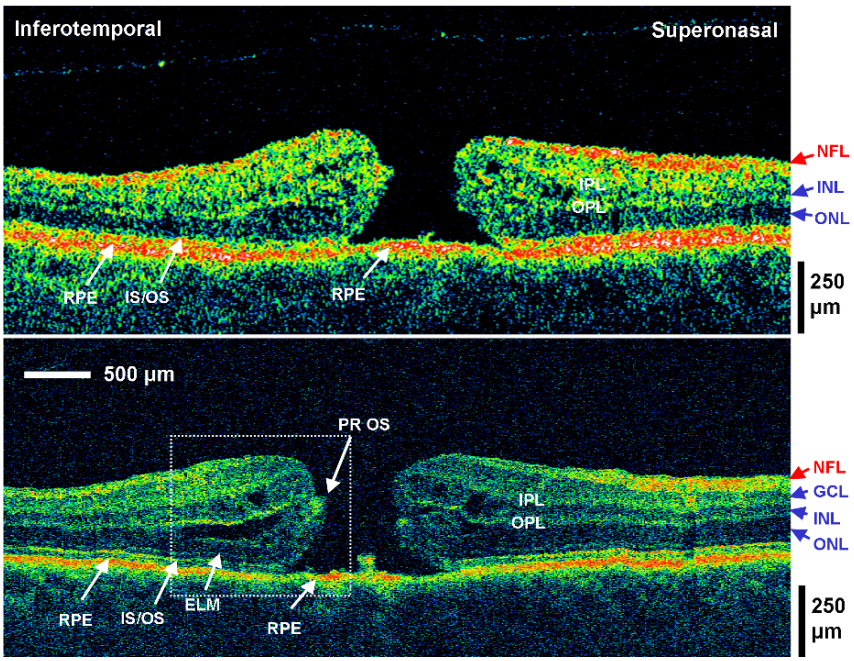

Fig. 1.11. Comparison of standard 10 µm and ultrahigh ∼3 µm resolution OCT retinal images of a full thickness macular hole. The ultrahigh-resolution OCT image shows that the photoreceptors are preserved in the region of the hole, even though they are lifted away from the retinal pigment epithelium. From ref [39]

either partial or full thickness disruption of normal retinal structure. Ultrahigh resolution OCT provides unprecedented axial resolution to visualize the intraretinal morphology of retinal diseases. These advances promise to improve our understanding of retinal disease pathogenesis.

Femtosecond Ti:Al_2O_3 lasers, in combination with high nonlinearity, air–silica microstructure fibers or tapered fibers, can generate a broadband continuum that spans the visible to the near-infrared wavelength range. These fibers have enhanced nonlinearity because of their dispersion characteristics, which shift the zero dispersion to shorter wavelengths, and the small core diameters, which provide tight mode confinement. High numerical aperture fibers have been used with femtosecond Ti:Al_2O_3 lasers to achieve bandwidths of up to 200 nm [40, 41]. Continuum generation from a femtosecond Ti:Al_2O_3 laser with air–silica microstructured photonic crystal fibers was demonstrated to achieve OCT image resolutions of 2.5 µm in the spectral region 1.2 to 1.5 µm [42], resolutions of 1.3 µm in the spectral region 800 to 1 400 nm [43], and record resolutions of <1 µm in the spectral region of 550 to 950 nm [44].

Although they have outstanding performance, femtosecond laser light sources are relatively costly and complex. Recent advances have demonstrated that Ti:Al_2O_3 lasers can operate with much lower pump powers than previously thought possible, thereby greatly reducing the cost of these lasers [45, 46]. At the same time, there have been advances in multiplexed SLD technology, and bandwidths approaching 150 nm can now be achieved, but with limited power [47]. Therefore, applications for very high-performance Ti:Al_2O_3 laser systems will likely be limited to research laboratories.

1.7 Ultrahigh-Resolution Imaging Using Cr:Forsterite Femtosecond Lasers

With the exception of the eye, most biological tissues are highly scattering. Since optical scattering decreases at longer wavelengths, wavelengths of 1 300 nm are used for most OCT imaging applications because they enable imaging deeper than shorter wavelengths, such as 800 nm [9–11]. Most commercial OCT systems at these wavelengths use SLD light sources that have bandwidths of ∼50 to 80 nm, thereby yielding axial image resolutions of ∼10 to 15 µm.

The KLM femtosecond Cr:Forsterite laser operates at wavelengths near 1 300 nm. The Cr:Forsterite laser material has lower gain than Ti:Al_2O_3, but has the advantage that it can be directly pumped at 1 µm wavelengths using compact Yb fiber lasers. The first OCT imaging studies using femtosecond Cr:Forsterite lasers performed many years ago demonstrated OCT axial image resolutions of 5 to 10 µm by coupling the femtosecond laser output into a nonlinear fiber and broadening the spectrum by self phase modulation [48]. Early Cr:Forsterite laser technology was challenging to use because the laser